Supporting Information

Assessment of 2,4-dinitroanisole transformation using compound-specific isotope analysis after in situ chemical reduction of iron oxides

Matthew J. Berens[†], Thomas B. Hofstetter[‡], Jakov Bolotin[‡], and William A. Arnold[*,†]

[†]Department of Civil, Environmental, and Geo-Engineering, University of Minnesota, 500 Pillsbury Drive SE, Minneapolis, Minnesota 55455-0116, United States

[‡]Eawag, Swiss Federal Institute of Aquatic Science and Technology, Department of Environmental Chemistry, Überlandstrasse 133, CH-8600 Dübendorf

[*]**Corresponding Author:**

William A. Arnold: arnol032@umn.edu

15 Pages, 7 Figures, 4 Tables, 1 Scheme

Contents

S1 CHEMICALS

Methanol (ACS grade), $NaHCO_3$ (ACS grade), and HCl (trace metals grade) were purchased from Sigma. 2,4-Dintroanisole (DNAN,98%) was purchased from Alfa Aesar. $FeCl_2$•$6H_2O$ (ACS grade), HCl (37%, ACS grade), NaOH (50% in H_2O), H_2SO_4 (ACS grade), acetonitrile (HPLC grade), ferrozine (B-(2-pyridyl)-5,6-bis(4-sulfophenyl)-1,2,4-triazine disodium salt hydrate, >98%), and NaCl (ACS grade) were purchased from Fisher. The DNAN transformation products 2-amino-4-nitroaniline (2-ANAN, 98%), 4-amino-2-nitroaniline (4-ANAN, 97%), and 2,4-diaminoanisole (DAAN, ≥98%) were purchased from Fisher.

All glassware, cuvettes, stir bars, and Nalgene bottles were soaked in 0.1 M oxalic acid (pH 3.5) for at least 2 days and rinsed with ultrapure water prior to use to remove any residual iron.

S2 ADDITIONAL DETAILS OF MINERAL CHARACTERIZATION

X-Ray diffraction (XRD) patterns were collected using a PANanalytical X'Pert Pro X-ray diffractometer equipped with a cobalt source (1.79 Å) and an X'Celerator detector. Scans were performed from 20° to 60° 2θ over 60 min and compared to powder diffraction files (PDF) No. 29-0713 (goethite), No. 33-0664 (hematite), No. 19-0629 (magnetite), and No. 46-1045 (quartz). Before analysis, each mineral was washed three times via centrifugation with ultrapure water to remove any salts, dried, and finely ground using a mortar and pestle. The relevant chemical properties of all materials are provided in Table S1. All collected XRD patterns are shown in Figure S1.

Table S1. Chemical properties of natural materials and the synthetic analogs* used in this study. Mineral phases were determined by X-ray diffraction (XRD).

sample	reactive iron phase	bulk mineral phase	total Fe % (w/w)	Fe(II)/Fe(III)
TCAAP	magnetite (Fe_3O_4)	quartz (SiO_2)	3.03[c]	<LOD
TCAAP extract[a]	magnetite (Fe_3O_4)	quartz (SiO_2)	6.9	0.1
magnetite*[a]	magnetite (Fe_3O_4)	n.d.[b]	72[d]	0.5
Tinker AFB	hematite (Fe_2O_3)	quartz (SiO_2)	2.04[c]	<LOD
hematite*	hematite (Fe_2O_3)	n.d.[b]	70[d]	<LOD

[a]data obtained from Strehlau et al.[1] [b]none detected. [c]Determined by ICP-OES. [d]estimated from structural formulas of pure minerals.

S3 ANALYTICAL METHODS

Ferrozine assay. The Fe(II) content was determined by the method of Viollier et al.[2] Aliquots from the batch reactors were extracted and filtered as described in the previous sections. To measure the Fe(II) content, 0.10 mL of reaction filtrate was transferred to clean, dry polystyrene cuvette with 2.70 mL deoxygenated, ultrapure water and 0.20 mL of a 5 g/L aqueous ferrozine solution. Each sample was capped, mixed by inversion, and the absorbance was measured at 562 nm using a Shimadzu UV-1601PC UV-Vis spectrophotometer. A five-point calibration curve was constructed by producing serial dilutions from 0.0–0.005 mM Fe(II) in ultrapure water. A ferrozine/ultrapure water solution was used as the blank. The Fe(III) content of a sample can also be quantified by the ferrozine assay as in the case of determining magnetite stoichiometry.

HPLC-DAD. Aqueous DNAN, MENA, iMENA, and DAAN concentrations were quantified with an Agilent Technologies 1200 Series HPLC equipped with a diode array detector (DAD) and an

Inertsil ODS-3 column (4.6 × 250 mm, 5 µm particle size). All analytes were detected at a wavelength of 230 nm. The mobile phase (60 % acetonitrile/40 % ultrapure water) was operated at a flow rate of 1.00 mL/min. The injection volume was 20 µL. A five-point calibration curve was produced for DNAN from 10–200 µM. The typical retention times with this method were approximately 3.1, 4.3, 5.7 min and 7.0 min for DAAN, iMENA, MENA, and DNAN, respectively.

SPME. Extraction of aqueous samples for compound specific isotope analysis (CSIA) was performed via online SPME carried out using a PAL autosampler equipped with a PAL SPME Arrow Tool and a Heatex Stirrer. All samples were initially diluted with 10 mM phosphate buffer (pH=7) to obtain concentrations within a range of linear response, and sodium chloride (200 g/L) was added to maximize extraction efficiency. Following equilibration at 50 °C for 10 min, the SPME Arrow was immersed in the sample for 70 minutes at 50 °C (600 RPM stir rate), and then DNAN was thermally desorbed from the arrow in an injector equipped with a deactivated liner (270 °C, 6 minutes).

GC/IRMS. DNAN $^{15}N/^{14}N$ and $^{13}C/^{12}C$ isotope ratios were determined using a Trace GC (Thermo Electron Corp.) coupled to an isotope ration mass spectrometer (IRMS; DeltaPLUS XL, Thermo Electron Corp.) via a combustion interface (GC Combustion III, Thermo) equipped with a Ni/Pt reactor. The GC contained an Rtx-5MS capillary column (0.32 mm ID, 1 µm film thickness, 30 m length) and was operated in splitless mode (splitless time 6 minutes, purge flow 50 ml/min) with the following temperature program: 50 °C for 1 minute, ramp 10 °C/min to 250 °C, hold for 5 minutes. During $\delta^{15}N$ analysis a liquid nitrogen trap was used to trap CO_2 produced from combustion. The self-made oxidation reactor was operated as described previously.[3] Method quantification limits (MQLs) for $\delta^{13}C$ and $\delta^{15}N$ signatures according to the moving mean procedure were 0.2 µM and 1 µM, respectively.[4]

Analytes were measured against standard laboratory gases that were introduced at the beginning of each run (CO_2 and N_2 for C and N isotope ratio measurements, respectively). Subsets of six samples were bracketed with DNAN standards in duplicate or triplicate to allow correction for any drift in signal observed during each run. The δ13C and δ15N values for the solid DNAN standard were determined to be -37.38 ± 0.01 ‰ and -2.48 ± 0.06 ‰, respectively, by EA/IRMS.

S4 ELECTRON BALANCE CALCULATIONS

Batch experiments. The total amount of electrons transferred from Fe-bearing materials to DNAN in batch reactors was calculated according to eq S1.

$$\text{total electrons transferred} = (6c_{MENA} + 6c_{iMENA} + 12c_{DAAN}) * V_R \quad (S1)$$

where V_R is the reactor volume (35 mL) and the analyte concentrations (*c*) are those at the endpoint of batch experiments.

Column experiments. In column experiments, the cumulative amount of electrons transferred were calculated by integrating the concentration measurements shown in Figures 2c-d according to eq S2.

$$\text{total electrons transferred} = \int_0^V (6c_{MENA} + 6c_{iMENA} + 12c_{DAAN})\text{dV} \quad (S2)$$

where *c* is the measured analyte concentration at the column outlet and V is the volume of DNAN solution introduced to the column.

S5 ADDITIONAL SEDIMENT COLUMN DETAILS

The physical properties of packed sediment columns are provided in Table S2. The calculation of dispersion coefficients (D) in columns was adapted from Kreft and Zuber[5] as shown in eq S3.

$$\frac{c}{c_0} = \frac{1}{2}\mathrm{erfc}\left(\frac{L - uz}{\sqrt{4Dz}}\right) + \frac{1}{2}\exp\left(\frac{uL}{D}\right)\mathrm{erfc}\left(\frac{L+uz}{\sqrt{4Dz}}\right) \quad (S3)$$

where c/c_0 is the normalized DNAN concentration at the column outlet relative to the input level, u is the mean flow velocity in the column, L is the column height, and z is the vertical displacement in the column. Because our measurements were made at the column outlet, L was equal to z in all cases. Fitting was performed using the Levenberg-Marquardt algorithm in Origin Version 2019b (OriginLab Corporation).

Table S2. Physical parameters of columns. Mean diffusion coefficients (D) determined from the nonreactive tracer were small and slightly greater for Tinker AFB (2.53(12) x 10^{-4} cm^2 s^{-1}) than TCAAP (2.37(22) x 10^{-4} cm^2 s^{-1}) columns. Similarly, large values of Pe (> 40) and uninhibited breakthrough of the nonreactive tracer (~1 PV) indicated convection-dominated regimes without preferential flow. All columns were 2.5 cm I.D. by 10 cm in length.

						before		after	
type	**column no.**	**mass (g)**	**ρ_p (g mL^{-1})**	**ρ_b (g mL^{-1})**	**PV (mL)**	**φ**	**D (cm^2 s^{-1})**	**φ**	**D (cm^2 s^{-1})**
TCAAP	1	47.7	2.64	1.59	11.9	0.40	2.69×10^{-4}	0.41	2.69×10^{-4}
	2	32.2	2.60	1.64	9.0	0.46	2.35×10^{-4}	0.46	2.35×10^{-4}
	3	40.2	2.76	1.64	10.0	0.41	2.11×10^{-4}	0.43	2.11×10^{-4}
Tinker	1	27.5	2.68	1.70	11.5	0.37	2.48×10^{-4}	0.37	2.48×10^{-4}
AFB	2	30.2	2.72	1.72	10.5	0.49	2.41×10^{-4}	0.50	2.41×10^{-4}
	3	33.1	2.70	1.68	10.7	0.48	2.70×10^{-4}	0.49	2.70×10^{-4}

S6 CSIA DATA PROCESSING

Carbon and nitrogen isotope signatures ($\delta^{13}C$, $\delta^{15}N$) were calculated according to eq S4 from measured $^{13}C/^{12}C$ and $^{15}N/^{14}N$ values.[3,6]

$$\delta^{h}E = \left(\frac{^{h}E/\ ^{l}E_{sample}}{^{h}E/\ ^{l}E_{reference}} - 1 \right) * 1000‰ \quad (S4)$$

where $^{h}E/^{l}E_{sample}$ and $^{h}E/^{l}E_{reference}$ are the ratios of the heavy (h) and light (l) isotopes of the element, E.

The correlation of N and C isotope fractionation ($\Lambda^{N/C}$) was determined using both simple linear regression and by the York model as described by Ojeda et al.[7] Linear regression analyses were performed in R (Version R-3.6.2) with RStudio (Version 1.2.5033) and the 'rgr' and 'IsoplotR' packages. The method and example R script are provided in the supporting information of Ojeda et al.[7]

S7 ADDITIONAL CSIA RESULTS

Bulk carbon and nitrogen isotope enrichment factors (ε_C and ε_N) and AKIEs were calculated from all experiments (Table S3). The values were obtained from experiments for DNAN reduction with untreated materials receiving a constant supply of 1 mM dissolved Fe(II). The predictions made by applying the Rayleigh fractionation equation (eq 4) to our results are shown in Table S4. Details of the calculations are provided in the main text.

Table S3. Bulk N and C isotope enrichment factors (ε_E) and AKIEs in batch reaction for DNAN reduction. All errors represent 95% confidence intervals. These values correspond to the data presented in Figure 3 in the main text.

material	ε_N (‰)	^{15}N-AKIE (-)	ε_C (‰)	^{13}C-AKIE (-)
Tinker AFB				
untreated + Fe(II)	-11.1 ± 4.3	1.023 ± 0.009	-0.7 ± 0.1	1.0007 ± 0.0002
reduced	-9.9 ± 3.8	1.020 ± 0.008	-0.2 ± 0.1	1.0002 ± 0.0002
hematite	-21.2 ± 3.3	1.044 ± 0.007	-0.3 ± 0.4	1.0003 ± 0.0008
TCAAP				
untreated + Fe(II)	-21.5 ± 2.6	1.045 ± 0.005	-0.8 ± 1.0	1.0008 ± 0.0020
reduced	-15.8± 4.3	1.033 ± 0.009	-0.3 ± 0.2	1.0003 ± 0.0004
magnetite	-13.2 ± 1.7	1.027 ± 0.003	-0.7 ± 0.3	1.0007 ± 0.0006
goethite[a]	-16.9 ± 3.0	1.035 ± 0.003	-0.1 ± 0.3	1.0000 ± 0.0003
mackinawite[a]	-18.8 ± 1.4	1.039 ± 0.001	-0.8 ± 0.6	1.0008 ± 0.0008

[a]data obtained from Berens et al.[8]

Table S4. Estimated values of predicted vs measured DNAN transformation in sediment columns. All errors represent 95% confidence intervals.

material	measured (c/c_o)	$\delta^{15}N$ (‰)	predicted (c/c_o)	error (c/c_o)
TCAAP	0.98	-1.94 ± 0.16	0.96± 0.010	0.02
	0.97	-1.52 ± 0.11	0.94 ± 0.007	0.03
	0.83	3.51 ± 0.15	0.67 ± 0.007	0.16
	0.50	9.59 ± 0.02	0.45 ± 0.001	0.04
	0.24	14.28 ± 0.16	0.33 ± 0.003	0.09
	0.15	16.64 ± 0.13	0.28 ± 0.002	0.13
	0.14	15.06 ± 0.43	0.31 ± 0.009	0.18
Tinker AFB	1.00	-2.22 ± 0.08	0.98 ± 0.005	0.02
	0.98	-1.20 ± 0.11	0.92 ± 0.007	0.06
	0.94	-1.04 0.91	0.91 ± 0.008	0.03
	0.41	8.47 ± 0.18	0.48 ± 0.006	0.07
	0.19	14.82 ± 0.11	0.32 ± 0.002	0.13
	0.16	11.95 ± 0.12	0.38 ± 0.003	0.22

S8 ADDITIONAL FIGURES.

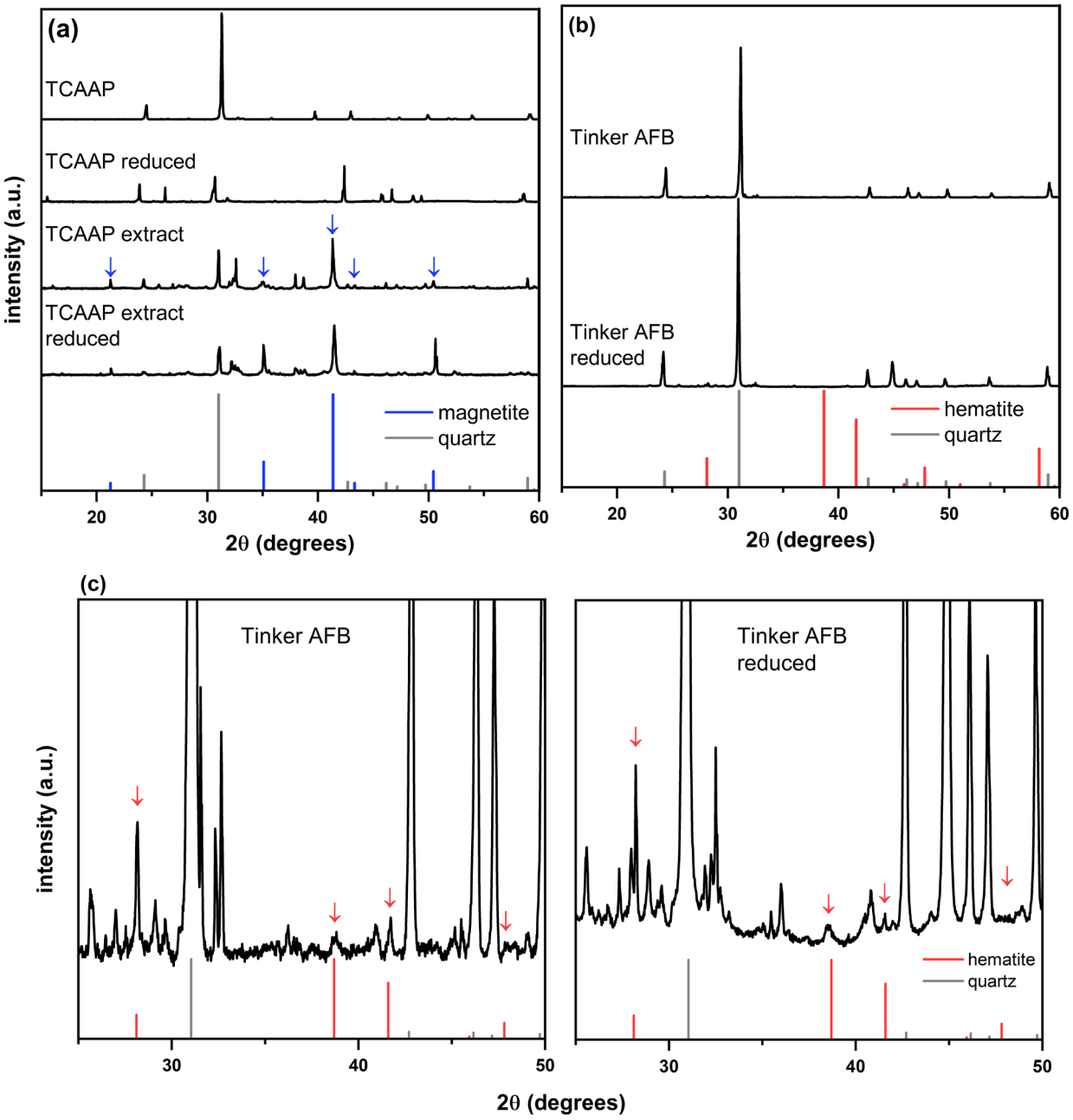

Figure S1. X-ray diffraction patterns of native and dithionite-reduced minerals used in this study. Both the bulk TCAAP material (a, top two patterns) and the magnetic extract (a, bottom two patterns) indicated that magnetite was the dominant iron-bearing mineral phase. (b) Hematite was the dominant iron phase in Tinker AFB sediment. Because of the strong quartz signal in Tinker AFB patterns, an enlarged subsection is provided in (c). These data reveal that negligible phase transformation occurred during ISCR and suggest that the primary effects of the treatment on the underlying mineralogy was the (re)generation of surface Fe(II).

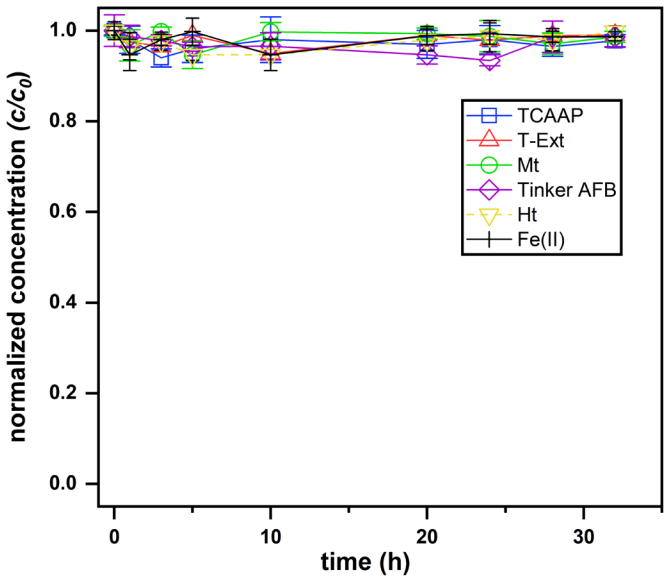

Figure S2. Control experiments for DNAN removal in suspensions of untreated minerals and dissolved Fe(II) without a mineral present. No reduction was observed over 32 h. Reactors remained on the rotator for three weeks with no detectable concentration loss (data not shown).

Scheme S1. Reductive transformation mechanism of DNAN to form 2/4-ANAN and DAAN. Each nitro-group transformation to form an amino-group requires the transfer of 6 electrons and 6 protons.

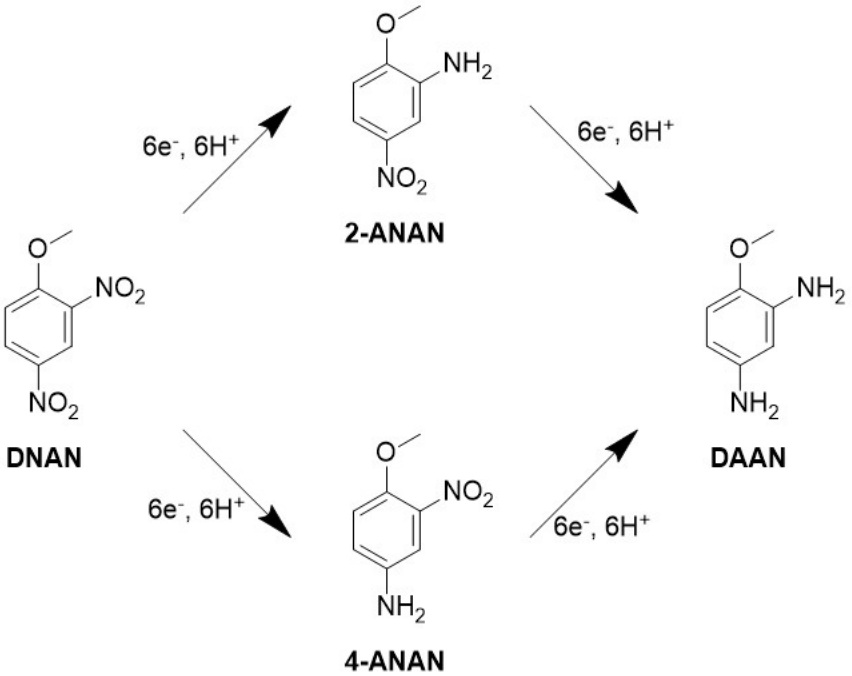

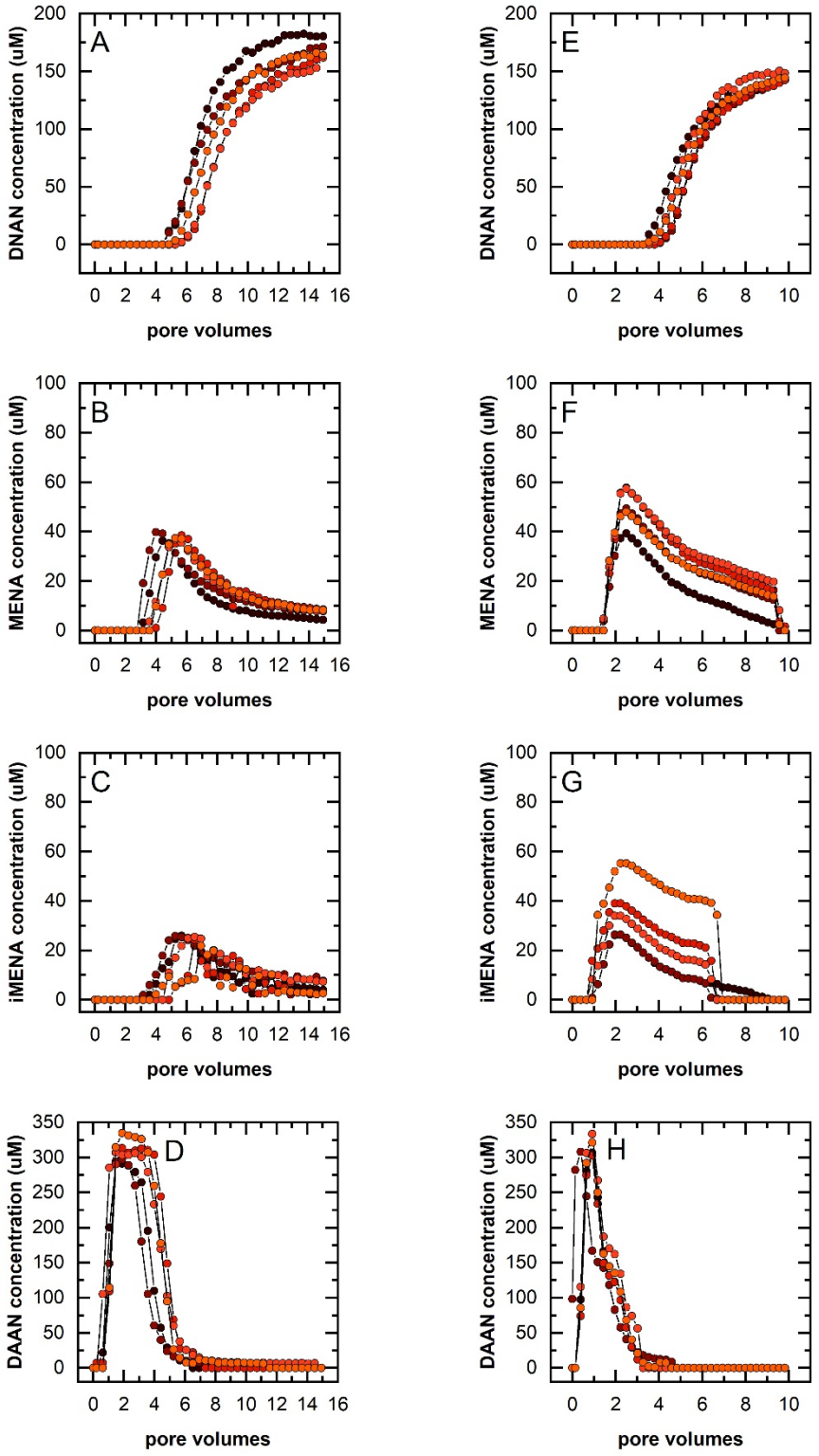

Figure S3. Breakthrough curves for 200 µM DNAN in (A-D) TCAAP and (E-H) Tinker AFB sediment columns following five sequential cycles of dithionite exposure and DNAN reduction. These are the data from Figure 2 (main text) expanded to show each individual cycle.

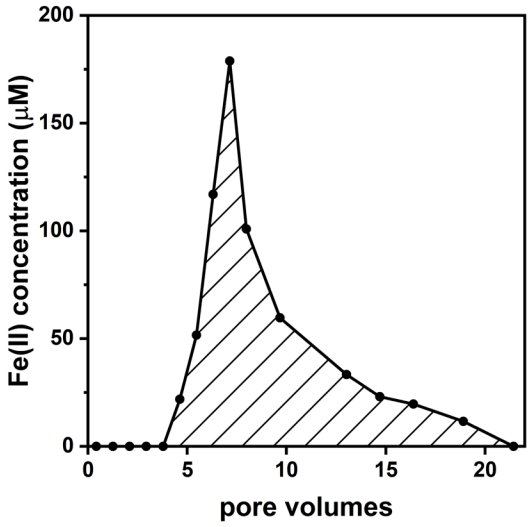

Figure S4. Representative concentration profile of Fe(II) detected in column effluents during dithionite treatment.

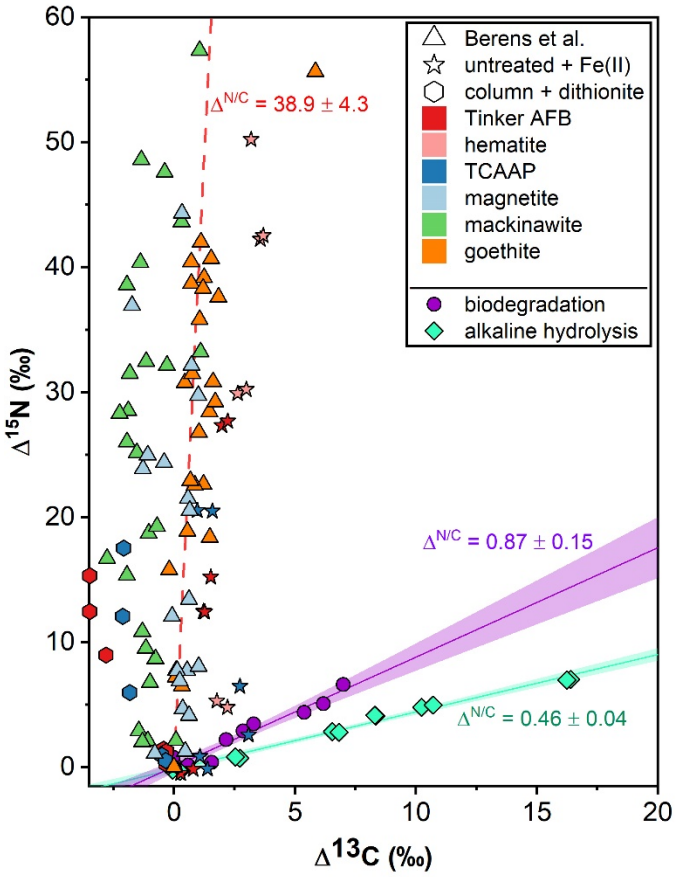

Figure S5. Dual-element (N vs C) isotope analysis to indicate multiple potential DNAN transformation pathways. Data from the present study for abiotic reduction by untreated minerals + Fe(II) (stars) and from columns receiving ISCR (hexagons) are shown. The observations from our previous work[8] is also provided (triangles). The dotted line represents the fit from linear regression by the York method as described by Ojeda et al.[7] The isotope fractionation observed during biodegradation (circles) and alkaline hydrolysis (diamonds) are provided for reference. The latter data sets were reproduced with permission from Ulrich et al.[9] Shaded portions represent the 95% confidence intervals from nonlinear regression analysis.

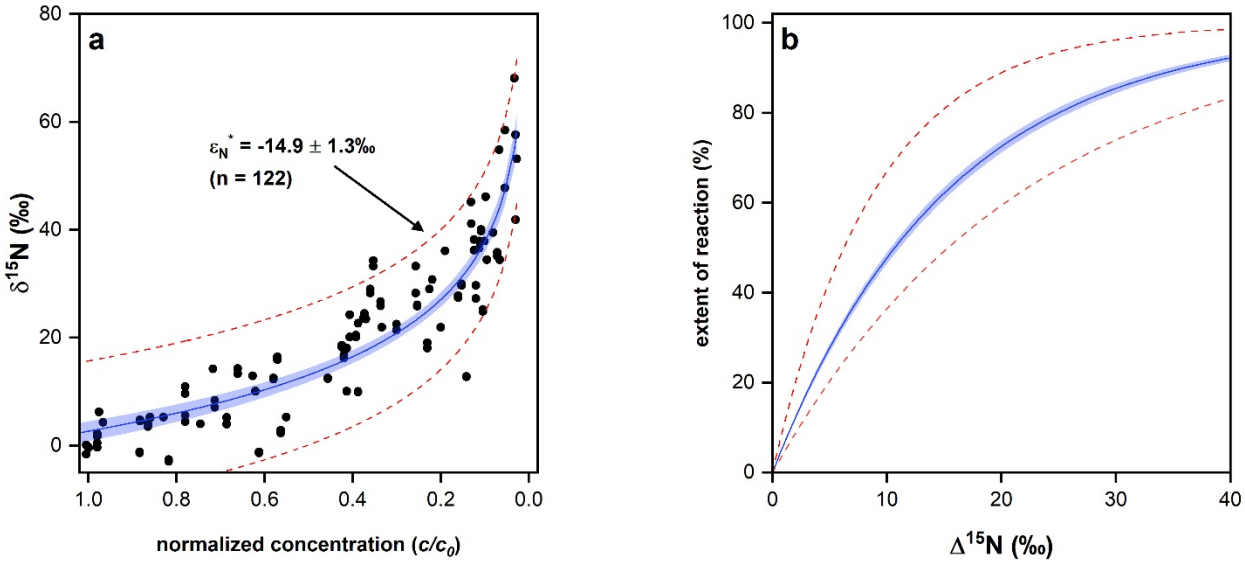

Figure S6. $\delta^{15}N$ vs c/c0 values were combined from all batch experiments to evaluate consistencies in fractionation and calculate the associated ε_N^* value. Theoretical plot relating the extent of DNAN transformation to measured $\delta^{15}N$ values using eq 2.

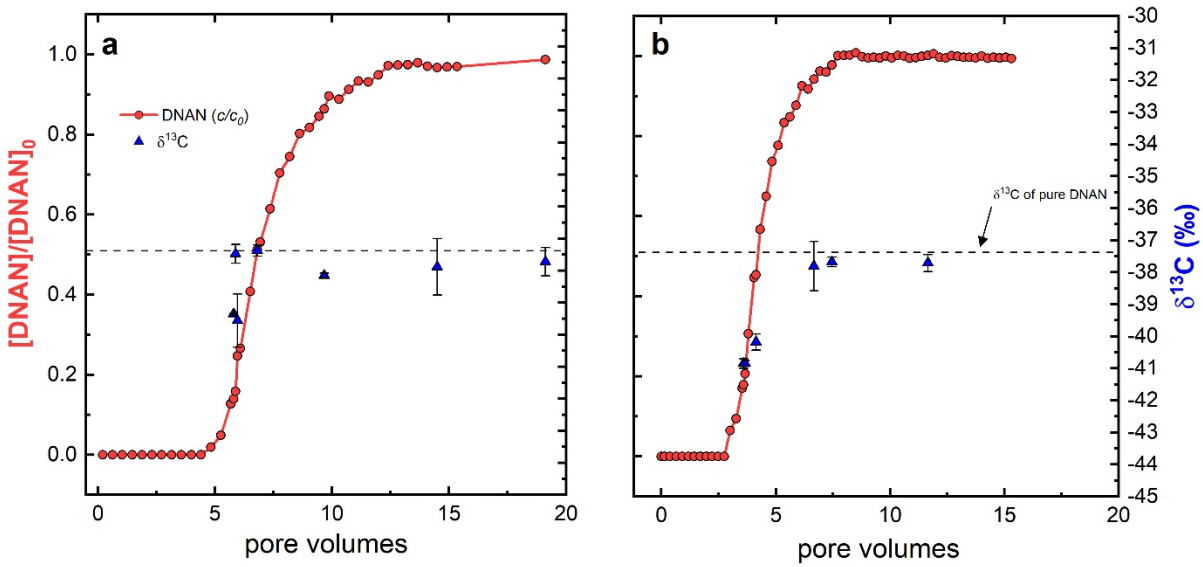

Figure S7. Extent of DNAN conversion ([DNAN]/[DNAN]$_0$, circles) and C isotope signatures ($\delta^{13}C$, triangles) measured at the breakthrough front during column experiments with dithionite-reduced (a) TCAAP and (b) Tinker AFB materials. Concentration data represent the average of five sequential breakthrough experiments. Error bars in $\delta^{13}C$ values indicate the standard deviations from triplicate measurements.

S9 REFERENCES

(1) Strehlau, J. H.; Berens, M. J.; Arnold, W. A. Mineralogy and Buffer Identity Effects on RDX Kinetics and Intermediates during Reaction with Natural and Synthetic Magnetite. *Chemosphere* **2018**, *213*, 602–609.

(2) Viollier, E.; Inglett, P. W.; Hunter, K.; Roychoudhury, A. N.; Van Cappellen, P. The Ferrozine Method Revisited: Fe(II)/Fe(III) Determination in Natural Waters. *Appl. Geochemistry* **2000**, *15* (6), 785–790.

(3) Spahr, S.; Huntscha, S.; Bolotin, J.; Maier, M. P.; Elsner, M.; Hollender, J.; Hofstetter, T. B. Compound-Specific Isotope Analysis of Benzotriazole and Its Derivatives. *Anal. Bioanal. Chem.* **2013**, *405* (9), 2843–2856.

(4) Spahr, S.; Bolotin, J.; Schleucher, J.; Ehlers, I.; von Gunten, U.; Hofstetter, T. B. Compound-Specific Carbon, Nitrogen, and Hydrogen Isotope Analysis of N -Nitrosodimethylamine in Aqueous Solutions. *Anal. Chem.* **2015**, *87* (5), 2916–2924.

(5) Kreft, A.; Zuber, A. On the Physical Meaning of the Dispersion Equation and Its Solutions for Different Initial and Boundary Conditions. *Chem. Eng. Sci.* **1978**, *33*, 1471–1480.

(6) Berg, M.; Bolotin, J.; Hofstetter, T. B. Compound-Specific Nitrogen and Carbon Isotope Analysis of Nitroaromatic Compounds in Aqueous Samples Using Solid-Phase Microextraction Coupled to GC/IRMS. *Anal. Chem.* **2007**, *79* (6), 2386–2393.

(7) Ojeda, A. S.; Phillips, E.; Mancini, S. A.; Sherwood Lollar, B. Sources of Uncertainty in Biotransformation Mechanistic Interpretations and Remediation Studies Using CSIA. *Anal. Chem.* **2019**, *91* (14), 9147–9153.

(8) Berens, M. J.; Ulrich, B. A.; Strehlau, J. H.; Hofstetter, T. B.; Arnold, W. A. Mineral Identity, Natural Organic Matter, and Repeated Contaminant Exposures Do Not Affect the Carbon and Nitrogen Isotope Fractionation of 2,4-Dinitroanisole during Abiotic Reduction. *Environ. Sci. Process. Impacts* **2019**, *21*, 51–62.

(9) Ulrich, B. A.; Palatucci, M.; Bolotin, J.; Spain, J. C.; Hofstetter, T. B. Different Mechanisms of Alkaline and Enzymatic Hydrolysis of the Insensitive Munition Component 2,4-Dinitroanisole Lead to Identical Products. *Environ. Sci. Technol. Lett.* **2018**, *5* (7), 456–461.